THE ASTROPHYSICAL JOURNAL, 322:812–821, 1987 November 15

THE INFRARED DIAGNOSTIC OF A DUSTY PLASMA WITH APPLICATIONS TO SUPERNOVA REMNANTS

ELI DWEK
Laboratory for Astronomy and Solar Physics, NASA-Goddard Space Flight Center
Received 1987 January 2; accepted 1987 May 14

ABSTRACT

IRAS observations of infrared emission from supernova remnants constitute the first observational evidence of shock-heated dust in the interstellar medium. These observations can provide valuable information on the morphology of supernova remnants, and on their interaction with the ambient interstellar medium. In particular, they can be used to study the physical condition and the cooling rate of dusty astrophysical plasmas. In this paper, I examine the possibilities and limitations of using the infrared observations as a diagnostic for the shocked gas, and as a means of determining remnant parameters. The paper presents improved calculations for the cooling rate of a dusty plasma by means of gas-grain collisions, and the equilibrium temperature of the dust for a variety of plasma conditions. These results are then used to define the density-temperature parameter space of the plasma, which, given its infrared spectrum, should be occupied by the observed remnant. This constraint can be used to estimate distances to supernova remnants and to set limits on various parameters that determine their evolution. The analysis is applied to the remnants Cas A and the Cygnus Loop.

Subject headings: infrared: sources — interstellar: grains — nebulae: supernova remnants — plasmas — radiation mechanisms

I. INTRODUCTION

The discovery of infrared emission from galactic supernova remnants (SNR; Braun 1987; Mufson *et al.* 1986; Dwek *et al.* 1987*a*, *b* [hereafter DPSR]) and from remnants in the Large Magellanic Clouds (Graham *et al.* 1987) by the Infrared Astronomical Satellite (*IRAS*) represents the first observational evidence for the collisional heating of dust in the interstellar medium. The only exception, so far, to this general statement is the Crab, where the dust is predominantly heated by the nonthermal radiation field in the nebula (Dwek and Werner 1981; Marsden *et al.* 1984; Mezger *et al.* 1986). This major discovery necessitates a careful reexamination of the collisional heating of dust and its effect on the cooling of the remnant.

The importance of infrared emission from collisionally heated dust to the cooling of a dusty plasma and to remnant evolution was recognized long before the *IRAS* observations by many authors including Spitzer (1968), Dalgarno and McCray (1972), Ostriker and Silk (1973), Burke and Silk (1974), Silk and Burke (1974), Draine and Salpeter (1979), Dwek and Werner (1981), Draine (1981), and Dwek (1981). Subsequent to these publications, new data have been made available on the stopping ranges of electrons in solids in the low-energy regime (Iskef, Cunningham, and Watt 1983). In addition, Draine and Lee (1984; see also Draine 1987) recently provided optical constants for astronomical-type silicate and graphite grains, which can be used to obtain more "realistic" values for the temperature of the radiating dust.

A major contribution of this paper, therefore, is in providing improved expressions for the infrared cooling rate of a dusty plasma, and for the temperature of the collisionally heated dust. The collisional heating rate of dust is presented in § II, and used in § III to derive the cooling function of a gas via gas-grain collisions for a variety of grain sizes and plasma conditions. In § IV the equilibrium dust temperature is calculated. The absolute value of the dust temperature may be uncertain by as much as 15%, and that of the cooling function by about a factor of 1.4. Particular emphasis is therefore placed on the qualitative behavior and dependence of these quantities under different plasma conditions. The results of these calculations show the limitations of determining plasma conditions from the infrared emission of collisionally heated dust. A clear distinction arises between the analysis of young remnants, characterized by postshock temperatures and velocities in excess of $\sim 2 \times 10^7$ K and ~ 1000 km s^{-1}, respectively, and the analysis of more evolved remnants that are expanding at lower velocities. This point is illustrated in § V, where these results are applied to the analysis of two remnants: Cas A, representing a young remnant; and the Cygnus Loop, representing a more evolved remnant. The conclusions of this paper are briefly summarized in § VI.

II. COLLISIONAL HEATING OF DUST

a) *The Collisional Heating Rate*

The electric potential on a dust particle embedded in a gas with temperatures above $\sim 10^6$ K is significantly smaller than kT (Draine and Salpeter 1979), so that the grain can be effectively treated as neutral. The heating rate of a dust grain of size a by ambient gas particles of mass m, number density n, and a Boltzmann distribution $g(E)$ of particle energies E at temperature T is then given by (e.g., Dwek 1986):

$$H(a, T, n) = \pi a^2 n \int g(E) v(E) E \zeta(a, E) dE$$
$$= (32/\pi m)^{1/2} \pi a^2 n (kT)^{3/2} h(a, T) , \quad (1)$$

where $g(E) = 2\pi^{-1/2}(kT)^{-3/2}E^{1/2} \exp(-E/kT)$, $v(E)$ is the velocity of the incident particle, and $\zeta(a, E)$ the fraction of the incident energy E that is deposited in the dust grain. The dimensionless quantity $h(a, T)$ is an effective grain "heating efficiency" given by (Dwek and Werner 1981):

$$h(a, T) = \tfrac{1}{2} \int x^2 \zeta(a, E = xkT) e^{-x} dx . \quad (2)$$

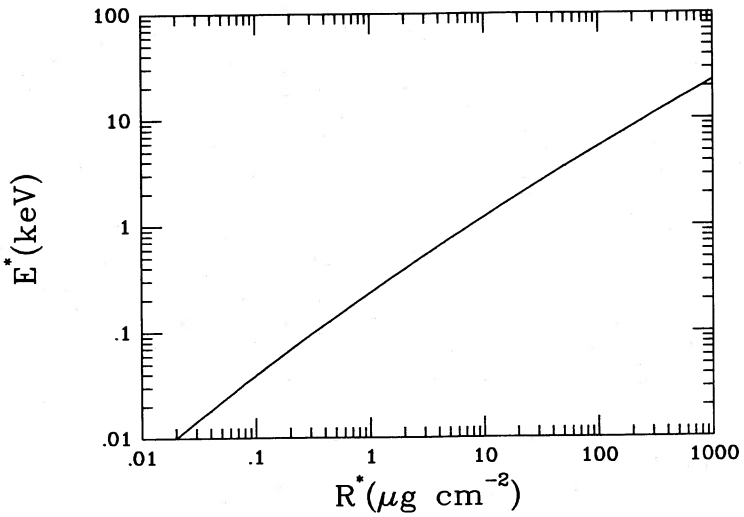

FIG. 1.—The value of E^*, the energy below which an incident electron is stopped in the grain, is shown here as a function of effective grain thickness R^*, which is given by $4a\rho/3$.

To calculate $\zeta(a, E)$ for various incident projectiles I will define a critical energy E^* as the energy at which the range of the incident projectile equals that of the dust particle. For an effective grain thickness of $4a/3$, the range, designated by R^*, is given by $4a\rho/3$, where ρ is the density (g cm^{-3}) of the dust grain. Projectiles with energy less than E^* have a large probability of being stopped in the grain, whereas projectiles with energies in excess of E^* have a large probability of penetrating the dust.

i) *Incident Electrons*

To calculate E^* I fitted the experimental ranges of electrons in all media within the energy range of 20 eV to 1 MeV (Iskef, Cunningham, and Watt 1983; Berger and Seltzer 1964) with the expression:

$$\log (R) = -8.150 + 0.502 \log (E) + 0.1466 \log^2 (E) , \quad (3)$$

where R is given in g cm^{-2}, and E is the electron energy in eV. This expression reproduces the best fit to the experimental data to within 15% over the entire energy range. The range of the electrons depends linearly on E between 20 and 400 eV, and has an $E^{1.75}$ dependence above 10 keV. The range in the above expression is the average value between the extrapolated range of the electrons, obtained by extrapolating the electron transmission curve versus target thickness to the abscissa, and the median range of the electrons, which represents the thickness of the absorber at which the fraction of transmitted electrons is reduced by a factor of 2. The two ranges are simply related to each other by a factor of 2.74 (Iskef, Cunningham, and Watt 1983). The value of E^* is then obtained by solving the quadratic equation for $R^* = 4a\rho/3$. Figure 1 depicts the solution for E^* as a function of effective grain thickness R^*.

Experimental data and Monte Carlo simulations of electron trajectories in solids (Janesick, Elliott, and Garmire 1985) suggest that a fraction of the incident electrons can escape a thick target. Therefore, even at energies less than E^*, $\zeta_e(E)$, the

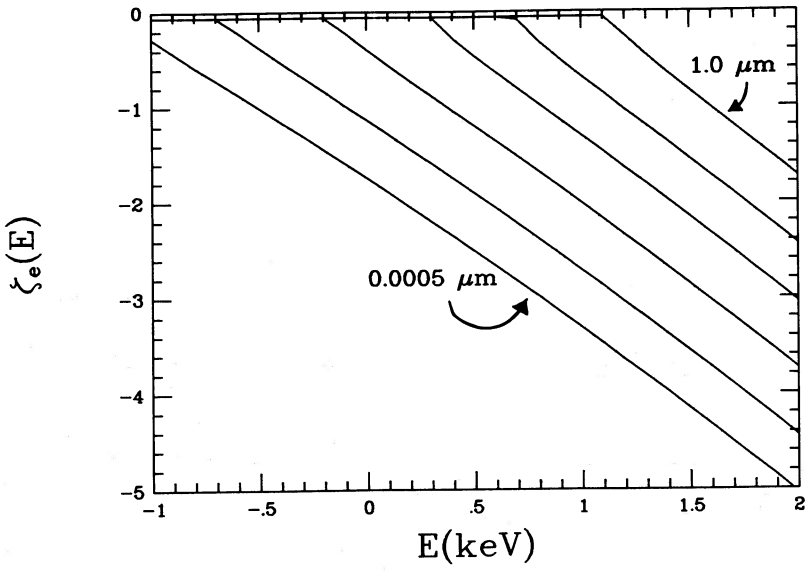

FIG. 2.—The fractional energy, $\zeta_e(a, E)$, deposited in a dust particle with a mass density of 3 g cm^{-3} is depicted here as a function of electron energy for 0.0005, 0.002, 0.01, 0.05, 0.2, and 1.0 μm size grains.

fraction of the incident electron energy that is deposited in the grains will be less than unity. Based on the experimental data, I adopted a value of $\zeta_e(E) = 0.875$ for $E < E^*$.

The fraction of the incident energy E deposited in the grain when $E > E^*$ is given by $(E - E')/E$, where E' is the final energy of the exiting electron given by the equation

$$R(E') = R(E) - R^* . \tag{4}$$

In practice, the final energy E' never falls below $0.125E$, since about 12.5% of the energy of the incident electrons always emerges as a result of their reflection from the grain surface. The prescription used for evaluating $\zeta_e(a, E)$ is then given by

$$\begin{aligned} \zeta_e(a, E) &= 0.875 && \text{for } E < E^* \\ &= (E - E_f)/E && \text{for } E > E^* , \end{aligned} \tag{5}$$

where $E_f = \max\{E', 0.125E\}$, and E^* is given in Figure 1.

Figure 2 shows the fractional energy deposited in a dust particle with a mass density of 3 g cm^{-3} as a function of electron energy for various grain sizes.

The grain heating efficiency for incident electrons was calculated by a numerical integration of equation (2). Figures 3*a* and 3*b* show the resulting values of $h_e(a, T)$ as a function of electron temperature for various sizes of graphite and silicate grains, respectively.

ii) *Incident Nuclei*

The fractional energy loss, $\zeta_n(E)$, from nuclei is given by (Dwek and Werner 1981)

$$\begin{aligned} \zeta_n(a, E) &= 1.0 && \text{for } E < E^* \\ &= E^*/E && \text{for } E > E^* . \end{aligned} \tag{6}$$

Draine and Salpeter (1979) presented analytical approximations to experimental stopping ranges of hydrogen in

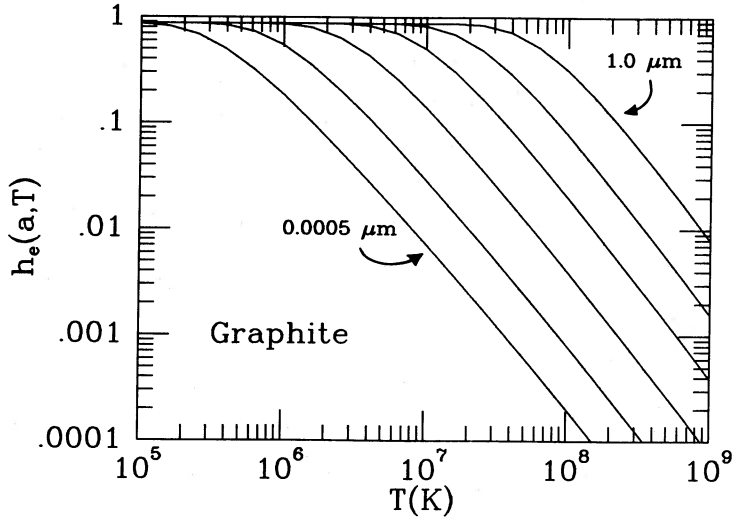

FIG. 3*a*

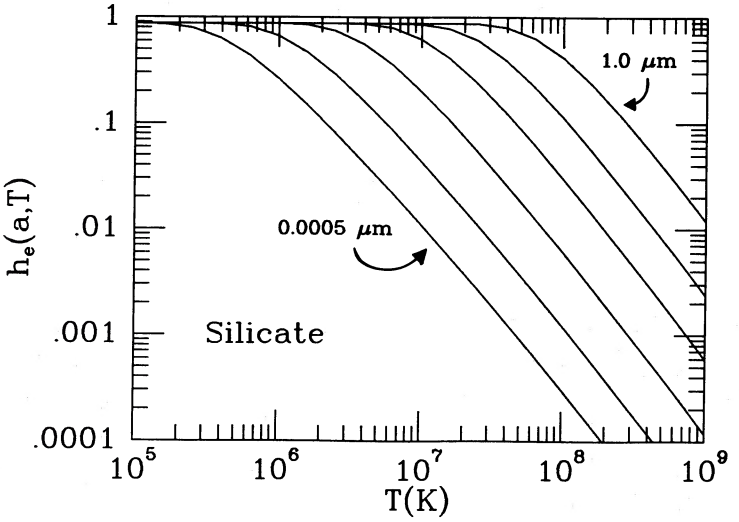

FIG. 3*b*

FIG. 3.—(*a*) The Planck-averaged value of the fractional electronic energy deposition in the dust, $h_e(a, T)$, is plotted as a function of electron temperature T, for 0.0005, 0.002, 0.01, 0.05, 0.2, and 1.0 μm size graphite grains. (*b*) The same as (*a*) for silicate grains.

various elements (Andersen and Ziegler 1977), which yield the following values for E^*:

$$\begin{aligned} E^*(\text{keV}) &= 133a(\mu\text{m}) \quad \text{H atoms} \\ &= 222a(\mu\text{m}) \quad \text{He atoms} \\ &= 665a(\mu\text{m}) \quad \text{CNO atoms} . \end{aligned} \tag{7}$$

The grain heating efficiency is given by the simple analytical expression

$$h_n(a, T) = [1 - (1 + E^*/2kT) \exp(-E^*/kT)] . \tag{8}$$

III. THE COOLING OF A DUSTY PLASMA

a) *The Infrared Cooling Function*

The cooling function of a dusty plasma (in ergs $\text{cm}^1\ \text{s}^{-1}$) by gas-grain collisions can be written as

$$\Lambda_d(T) = n_d \int H(a, T, n) f(a) da / n_e n_{\text{H}} , \tag{9}$$

where n_d is the number density of dust particles in the gas, $f(a)$ is the grain size distribution function (normalized to unity) in the $\{a_1, a_2\}$ size interval, and n_e and n_{H} are, respectively, the electron and hydrogen number density of the gas. For a dust-to-gas mass ratio, Z_d, the number density of dust grains is given by

$$n_d = [\mu m_{\text{H}} n_{\text{H}} / \langle m_d \rangle] Z_d \tag{10}$$

where μ is the atomic weight of the gas (in amu), m_{H} is the mass of a hydrogen atom, and $\langle m_d \rangle = 4\pi\rho/3 \int a^3 f(a) da$, the size-averaged mass of the dust.

An interstellar dust model that has been extremely successful in modeling the interstellar extinction curve was presented by Mathis, Rumple, and Nordsieck (1977; hereafter MRN). However, *IRAS* observations of high latitude "cirrus" clouds (Low *et al.* 1984), and their theoretical interpretation (e.g., Puget, Leger, and Boulanger 1985; Draine and Anderson 1985; Weiland *et al.* 1986) suggests that the MRN grain model should extend to very small grain sizes. The presence of these very small dust particles is also suggested by the "excess" 12 μm emission observed in the spectrum of Cas A (Dwek *et al.* 1987*a*). In calculating $\Lambda_d(T)$, I therefore adopted an "extended" MRN dust model characterized by a mixture of graphite and silicate particles with a $k = -3.5$ power-law in grain sizes from $a_1 = 0.001$ to $a_2 = 0.5$ μm, and a dust-to-gas mass ratio of 0.0075.

Figure 4 shows the resulting value of $\Lambda_d(T)$, plotted as a function of gas temperature T, for: the "extended" MRN interstellar dust model (curve a); a silicate-graphite mixture of 0.4 μm dust particles (curve b); a silicate-graphite mixture of 0.1 μm dust particles (curve c); and a silicate-graphite mixture of 0.01 μm dust particles (curve d). Curve (e) is the cooling function of the gas, $\Lambda(T)$, due to atomic processes (e.g., Raymond, Cox, and Smith 1976; calculated here using the latest equilibrium coronal plasma model of Raymond and Smith) and is included in the figure for sake of comparison.

b) *The Infrared-to-X-Ray Cooling Ratio*

The relative importance of gas cooling by infrared emission from dust, and by atomic processes (free-free, bound-free, and bound-bound transitions) can be expressed by the ratio of the respective cooling functions (curves a and e) given in Figure 4. This dust-to-gas cooling ratio, γ, is thus defined as

$$\gamma(T) = \Lambda_d(T)/\Lambda(T) . \tag{11}$$

For a given dust model and plasma that is in ionization equilibrium, the ratio γ is only a function of the gas temperature T.

Figure 5 depicts the value of γ as a function T. The relative importance of the two distinct cooling processes can be assessed by comparing the observed infrared and X-ray fluxes emitted from a remnant (see DPSR). The value of $\gamma(T)$ derived from the observations can deviate significantly from the theoretically predicted value depicted in Figure 5. Observed values significantly below the theoretical curve may suggest one or more of the following (1) the dust is significantly destroyed in the postshock gas; (2) the remnant is expanding into a medium with a lower than average dust-to-gas mass ratio; (3) the dust is

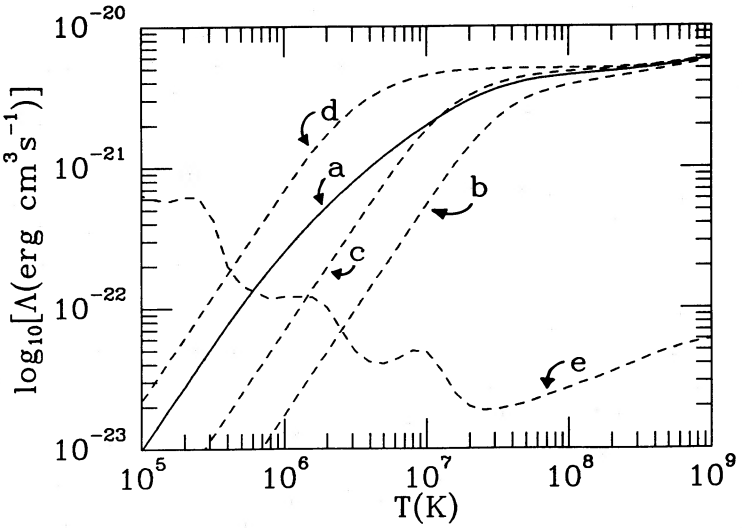

FIG. 4.—The cooling function of the gas via gas-grain collisions, $\Lambda_d(T)$, plotted as a function of gas temperature T, for: the "extended" MRN interstellar dust model (*curve a*); a silicate-graphite mixture of 0.4 μm dust particles (*curve b*); a silicate-graphite mixture of 0.1 μm dust particles (*curve c*); and a silicate-graphite mixture of 0.01 μm dust particles (*curve d*). Curve (*e*) is the cooling function of the gas, $\Lambda(T)$, due to atomic processes (Raymond, Cox, and Smith 1976) and is included in the figure for sake of comparison.

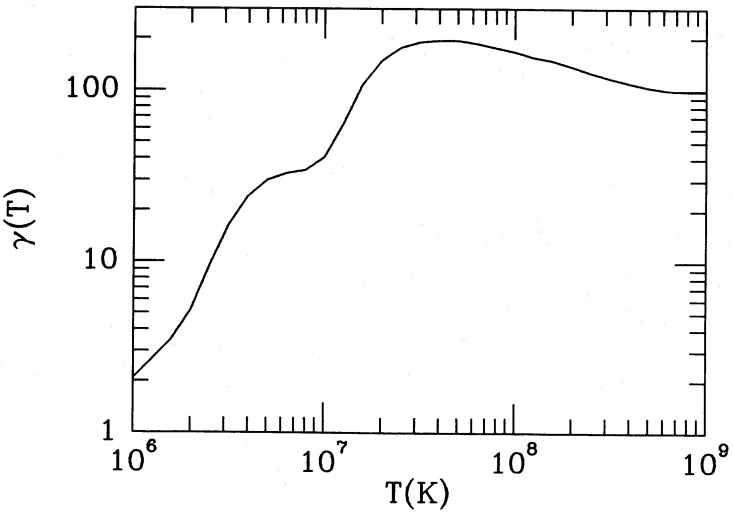

FIG. 5.—The parameter $\gamma(T)$, defined as the ratio between the cooling function of the gas via gas-grain collisions and that of the gas via atomic processes, $\Lambda_d(T)/\Lambda(T)$, is plotted here as a function of gas temperature T.

not well coupled to the gas in the postshock region. Derived values of $\gamma(T)$ that are significantly higher than the theoretical curve may suggest one or more of the following (1) the presence of density inhomogeneities (clumps) in the shocked gas. The shocks in these clumps are radiative shocks so that a significant fraction of the cooling of the gas is shifted outside the 0.2–4 keV X-ray band; (2) infrared lines contribute significantly to the emission in the *IRAS* bands; (3) a significant fraction of the infrared emission originated from radiatively heated dust. An agreement between the derived and the theoretical value of $\gamma(T)$ should, however, be treated with caution, since a combination of the various effects listed above may conspire to produce such a fit. In any case, a comparison between the infrared and X-ray fluxes from a remnant is extremely valuable in obtaining information on its evolution and interaction with the ambient interstellar medium.

IV. DUST TEMPERATURE

a) *Dust Cooling*

Dust particles with sizes below a certain critical size will be stochastically heated by the ambient plasma (Dwek 1986)—that is, a single electronic collision will cause a sudden surge in dust temperature, which is followed by a cooling period until the next collision. Larger grains, however, will have a well-defined temperature that is obtained by equating the dust cooling rate by infrared emission to its collisional heating rate. The cooling rate of a dust particle of size a is given by

$$L_{gr}(a, T_d) = 4\pi a^2 \sigma T_d^4 \langle Q(a, T_d) \rangle , \qquad (12)$$

where σ is the Stefan-Boltzmann constant, T_d is the dust temperature, and $\langle Q(a, T_d) \rangle$ is the Planck-averaged value of the dust absorption coefficient $Q_\lambda(a)$. For most remnants T_d is less than ~ 100 K. In this temperature region the value of $\langle Q(a, T_d) \rangle / a$ depends weakly on grain size and is given (in units of cm^{-1}), for less than or equal to 0.2 μm size graphite grains by

$$\langle Q(a, T_d) \rangle / a = 0.18 T_d^{1.92} , \quad 10 \le T_d \le 50$$
$$= 5.85 T_d^{1.04} , \quad 50 \le T_d \le 100 , \qquad (13a)$$

and for less than or equal to 0.2 μm size silicate grains by

$$\langle Q(a, T_d) \rangle / a = 0.126 T_d^2 , \quad T_d \le 100 . \qquad (13b)$$

It is useful to define the size-independent quantity $\langle K(T_d) \rangle = \langle 3Q(a, T_d)/4\rho a \rangle$ which is the Planck-averaged value of the mass absorption coefficient (units of mass/area) of the dust. The luminosity of a dust particle can then be conveniently expressed as

$$L_{gr}(a, T_d) = 4 m_{gr}(a) \sigma T_d^4 \langle K(T_d) \rangle \qquad (14)$$

where $m_{gr}(a) = 4\pi\rho a^3/3$ is the mass of a grain.

b) *Variation of Dust Temperature with Plasma Conditions*

The equilibrium temperature of a dust particle of size a is then determined by the equation

$$L_{gr}(a, T_d) = H(a, T, n) . \qquad (15)$$

Figure 6*a* depicts the temperature of an 0.1 μm silicate and graphite grain collisionally heated by a plasma with a total number density of 1 cm^{-3}. Subsequent figures (Figs. 6*b–d*) show the dependence of dust temperature, T_d, on total gas density, n, gas temperature, T, and grain size, a. Figure 6*b* depicts the temperature of a 0.1 μm size graphite particle as a function of n for several values of T. The dust temperature scales with density as $n^{0.20}$, and a similar plot for silicates yields an $n^{0.17}$ density dependence for silicate grains. This dependency of dust temperature on gas density simply reflects, respectively, the λ^{-1}, and the λ^{-2} behavior of $Q_\lambda(a)$ at long wavelengths. Figure 6*c* depicts the value of T_d (for an 0.1 μm sized graphite grain) as a function of T for various values of the gas density, and Figure 6*d* shows how the temperature of graphite particles varies with grain size for various values of T, and $n = 1$ cm^{-3}. At gas temperatures below $\sim 10^7$ K most of the grains are thick to the impinging electrons and $H \sim a^2$. Since $L_{gr} \sim a^3$, the dust temperature will depend on grain size as a^{-p}, with $p \approx 0.17$–0.20. As the gas temperature increases and the grains become transparent to the incident electrons $h_e(a, T) \sim a$, and the dust temperature becomes less dependent on grain size.

As will be discussed in detail in the following sections, these figures, combined with infrared observations, can provide a good estimate of the range of plasma conditions that prevail in the shocked gas.

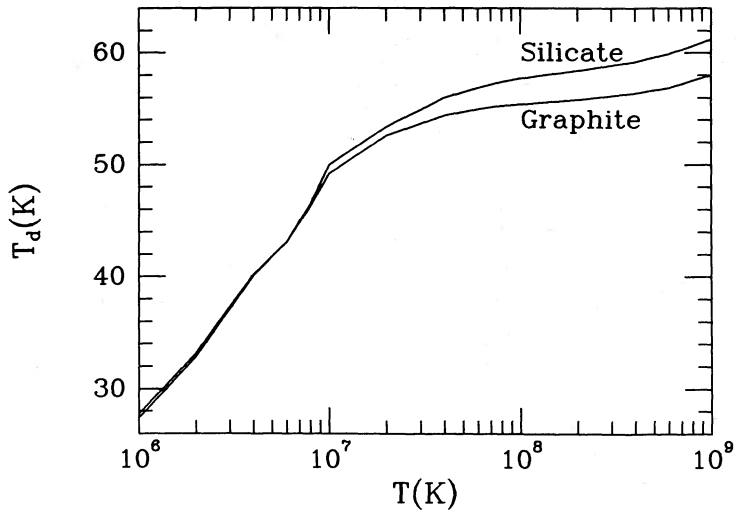

FIG. 6a

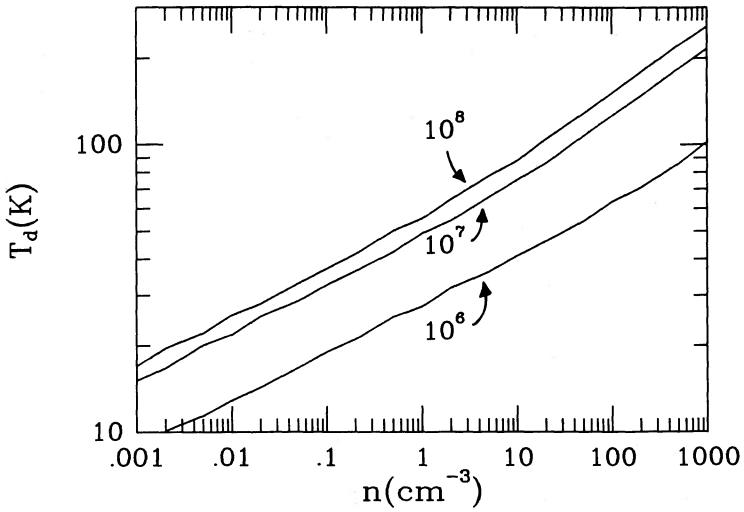

FIG. 6b

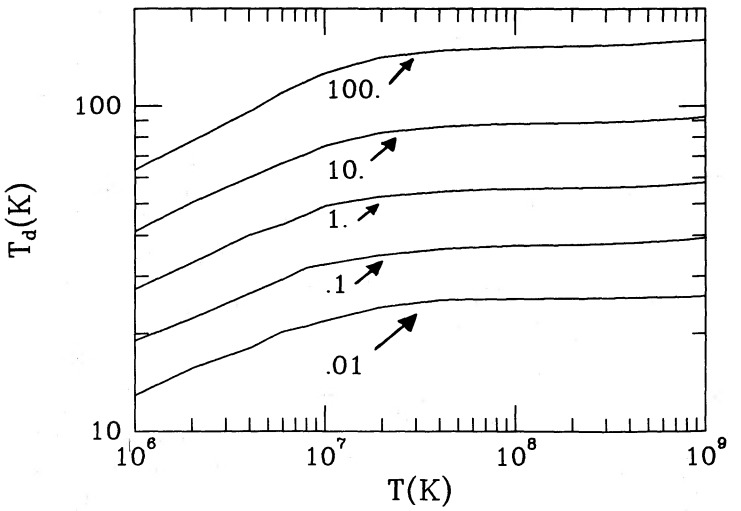

FIG. 6c

FIG. 6.—(*a*) The temperature of 0.1 μm silicate and graphite grains is depicted as a function of gas temperature T, for a gas density of $n = 1$ cm^{-3}. (*b*) The temperature of a 0.1 μm size graphite particle is shown here as a function of n for various values of the T(K). (*c*) The temperature of a 0.1 μm size graphite particle is shown here as a function of T for various values of n(cm^{-3}). (*d*) The variation of the temperature of a graphite grain as a function of grain size is shown here for $n = 1$ cm^{-3}, and for various values of T(K).

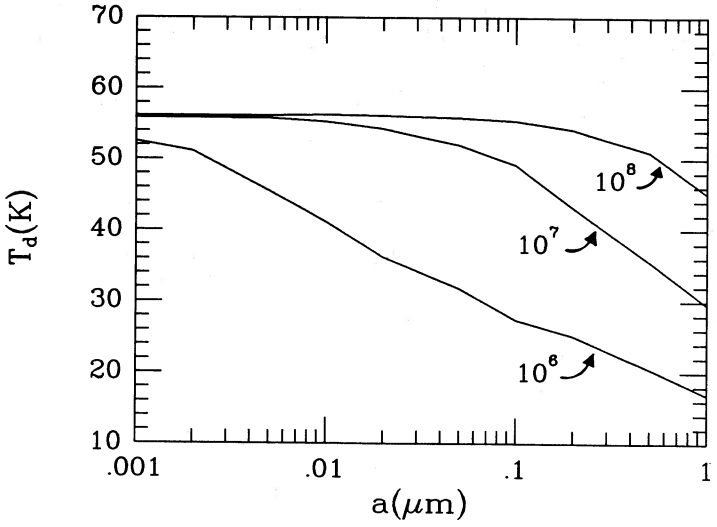

FIG. 6d

V. APPLICATIONS TO SUPERNOVA REMNANTS

In the following I will use the *IRAS* observations and the results derived in the previous sections to determine the plasma conditions and various parameters of the remnants Cas A and the Cygnus Loop. Given the dust temperature, the most reliably determined quantity is the density of the shocked gas in young remnants. The determination of remnant radius (or distance) and mass of swept-up gas are more uncertain since it requires the knowledge of two additional parameters. The first is related to the morphology and density-temperature structure of the remnant, and the second is related to the destruction of dust in shocks. In spite of the uncertainties in these parameters, the method is quite successful in deriving plasma conditions and remnant parameters for Cas A and the Cygnus Loop that are consistent with other observations.

a) Determination of Remnant Parameters

i) *Postshock Temperature and Density*

General conclusions on the physical condition of the shocked gas can be drawn from a simple inspection of the infrared spectrum of a remnant. Several remnants with postshock temperatures $T_s \geq 10^7$ K have a spectrum that can be very well approximated by a single dust temperature. An example is Cas A, which has an ~ 90 K spectrum, except for an excess emission at 12 μm, which is probably the result of temperature fluctuations of small particles (Dwek *et al.* 1987*a*). This fact alone suggests that the gas temperature in these remnants must be in excess of $\approx 10^7$ K; otherwise their infrared spectrum would be significantly broadened by the different dust temperature component associated with the different grain sizes (see Fig. 6*d*). These general considerations suggest that young remnants should have infrared spectra that can be characterized by a single dust temperature, whereas the older remnants will have significantly broader spectra reflecting a wider range of dust temperatures. A preliminary comparison of the spectra from Cas A (Braun 1987; Dwek *et al.* 1987*a*), Kepler and Tycho (Braun 1987; Dwek, Szymkowiak, and Petre, in preparation) with that of the more evolved remnant, the Cygnus Loop, supports this general statement.

More quantitative conclusions can be drawn from the detailed behavior of dust temperature in various plasma conditions. Figure 7 is a diagram depicting contours of constant dust temperature (calculated for an 0.1 μm graphite particle) as a function of gas density and temperature. The diagram has two shaded areas, one enclosed between dust temperatures of 85 and 95 K, the other between 30 and 35 K. The first area depicts the region in the (n, T) plane where we can expect to find young supernova remnants, such as Cas A, Tycho, or Kepler, whereas the second area corresponds to the region that will be occupied by older remnants, such as the Cygnus Loop. The diagram shows that the dust temperature can put useful constraints on gas density in young remnants but is a rather flat function of gas temperature. *Infrared observations alone can therefore not provide any constraints on shock velocities above* ~ 1000 *km* s^{-1}.

For older remnants, in which T is less than or equal to 2×10^7 K, the dust temperature provides a constraint on the allowable combinations of gas density and temperature behind the shock. Draine (1981), in an analysis of the infrared emission from shocks, presented an analytical expression between the wavelength of the peak intensity of the infrared spectrum and shock velocity. This expression, a result of the fundamental relation between dust temperature and gas temperature given in Figure 7, is *valid only for shock velocities below* ~ 1000 *km* s^{-1}. It should, however, be used with some caution, since dust temperature fluctuations can shift the position of the peak of the emission with respect to its location in the various models in Draine's paper.

ii) *Remnant Size and Distance*

The basic equation from which the remnant parameters can be deduced relates the total infrared luminosity of the remnant to the integral of $n_e n_H \Lambda_d(T)$ over its shocked interior. This energy balance equation can be written as

$$F_{IR} = 4\pi\delta \int_0^{R_s} n_e(r) n_H(r) \Lambda_d(T) r^2 dr / 4\pi D^2 , \qquad (16)$$

where r is the distance from the center of the explosion, R_s is the shock radius, δ is a factor (≤ 1) that accounts for the possible depletion of dust in the remnant, and D is the remnant's distance. Without loss of generality equation (16) can be written as

$$F_{IR} = 4\pi R_s^3 n_0^2 \delta \Lambda_d(T_s) \beta / 4\pi D^2 , \qquad (17a)$$

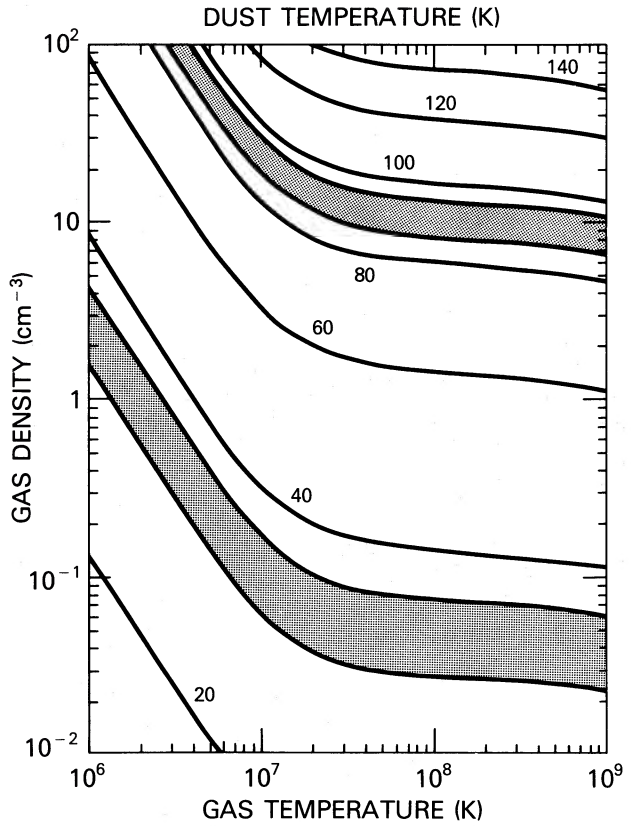

FIG. 7.—A diagram depicting contours of constant dust temperature (calculated for an 0.1 μm graphite particle) as a function of gas density and temperature. The diagram has two shaded areas: the first, enclosed between dust temperatures of 85 to 95 K, depicts the region in the (n, T)-plane where we can expect to find young supernova remnants, like Cas A or Tycho. The second area depicts the region in the (n, T)-plane that may be occupied by older remnants like the Cygnus Loop.

or

$$R_s = F_{IR}/[\delta\beta\Theta_R{}^2 n_0{}^2 \Lambda_d(T_s)] , \tag{17b}$$

where n_0 is the total number density of the ambient ISM, T_s is the postshock temperature, Θ_R is the angular radius of the remnant, and the parameter β is defined as

$$\beta = n_0{}^{-2} \int_0^1 n_e n_H [\Lambda_d(T)/\Lambda_d(T_s)] x^2 dx , \tag{18}$$

where $x = r/R_s$ is the dimensionless distance from the center of the explosion.

The calculation of β requires a knowledge of the morphology and evolutionary phase of the remnant and can be readily calculated if the remnant expands into a uniform medium. In the initial stages after the explosion, the ejecta expands almost freely into the ambient medium. The swept-up interstellar gas is confined to a narrow shell behind the shock, with the expanding ejecta dominating the temperature and density structure throughout most of its interior. However, the infrared emission is largely confined to the immediate postshock region which is also the first to relax to the adiabatic solution. Without any significant loss of accuracy, I can therefore assume that the immediate postshock density and temperature profiles are described by the adiabatic Sedov (1959) solution. Assuming a T^k dependency of $\Lambda_d(T)$ on gas temperature, the parameter β can be written as

$$\beta = \beta(k) = \int_0^1 f^2(x) h^k(x) x^2 dx , \tag{19}$$

where $f(x)$ and $h(x)$ are scaling functions that respectively describe the density and temperature profiles throughout the interior of the remnant and can be approximated by (Taylor 1950)

$$f(x) = 4x^{9/2}[1 + 3/5(1 - x^5)]^{-5/2}$$

and

$$h(x) = x^{-9/2}[1 + 3/5(1 - x^5)]^{-1/6} . \tag{20}$$

The value of β is difficult to estimate if the remnant expands into a clumpy medium. Assuming that all the clumps are characterized by the same density and temperature, n_c and T_c, respectively, $\beta(=\beta_c)$ can be written as

$$\beta_c = 1/3 f_c (n_c/n_0)^2 [\Lambda_d(T_c)/\Lambda_d(T_s)] , \tag{21}$$

where f_c is the volume filling factor (≤ 1.0) of the clumps in the remnant.

An additional parameter needed to calculate the remnant radius is δ, the depletion factor of the dust in the postshock gas. Detailed calculations on the destruction of dust particles in a hot gas were presented by Draine and Salpeter (1979), and more recently by Seab (1986). The results show that for gas temperatures above $\sim 10^6$ K, the lifetime of the dust against destruction by sputtering is given by $\tau(a) \approx 10^6 a(\mu m)/n$ yr, where $a(\mu m)$ is the grain radius in microns, and n the gas density in cm^{-3}. Since most of the mass of the shocked gas and dust is confined to the outer $\sim 10\%$ of the remnant's radius, this lifetime should be compared to the time it takes the dust to cross this region. The latter time is equal to $\sim t/3$, where t is the age of the remnant. The mass depletion factor is therefore approximately given by

$$\delta \approx \max \{0, 1 - 1 \times 10^{-6} nt(\mathrm{yr})/\langle a(\mu m)\rangle\} , \tag{22}$$

where $\langle a\rangle$ is the mass-averaged size of the dust in the remnant.

If the values of β and δ can be estimated with a reasonable degree of accuracy, equation (17b) can be used to determine the radius of the remnant (or alternatively, its distance) on the basis of the infrared emission alone. For simplicity, I will assume in the following that the remnant expands into a uniform medium. In young remnants with $T_s \geq 3 \times 10^7$ K, the cooling function is almost constant with gas temperature and has an average value $\Lambda_d(T) \approx 5 \times 10^{-21}$ ergs cm^3 s^{-1}, with $\beta(k = 0) = 0.694$. For older remnants with $10^6 \leq T_s \leq 3 \times 10^7$ K, $\Lambda_d(T) = 4.7 \times 10^{-27} T^{0.8}$ ergs cm^3 s^{-1}, and $\beta(0.8) = 0.840$. The radius of a remnant that is expanding into a uniform medium can therefore be written as

$$R_s(\mathrm{pc}) = 1.1 \times 10^9 F_{IR}/[\delta\Theta_R{}^2 n_0{}^2] \quad \text{for } T_s \geq 2 \times 10^7 \text{ K}$$

and

$$R_s(\mathrm{pc}) = 1.54 \times 10^{10} F_{IR} T_6{}^{-0.8}/[\delta\Theta_R{}^2 n_0{}^2] \quad \text{for } T_s \leq 2 \times 10^7 \text{ K} . \tag{23}$$

The infrared flux in equation (23) is given in units of (ergs s^{-1} cm^{-2}), and Θ_R is given in arcmin.

The equations derived above assume that the dust and gas are well coupled in the postshock region by confining magnetic fields. The validity of this assumption requires the Larmor radius of the dust to be small compared with the density scale

length behind the shock (e.g., Shull 1977). The Larmor radius of a charged dust grain in a magnetic field B is given by:

$$r_L(\mathrm{pc}) = 0.12\rho(a/0.1\ \mu\mathrm{m})^2 B^{-1}(\mu\mathrm{G}) U^{-1}(\mathrm{Volt}) \times (v_{\mathrm{gr}}/1000\ \mathrm{km\ s^{-1}}) f^{-1}\ , \quad (24)$$

where $U(\mathrm{Volt}) = 1.44 \times 10^{-3}\ Z_{\mathrm{gr}}/a(\mu\mathrm{m})$ is the grain potential (Z_{gr} is the grain charge in units of electron charge), v_{gr} is the grain velocity, and f is a compression factor ~ 4 in adiabatic shocks. For shock velocities of ~ 4000 km s^{-1}, $U \approx 10$ Volt (Draine and Salpeter 1979), and for $B = 1(\mu\mathrm{G})$, $r_L \approx 0.027$ pc. The density scale length behind adiabatic shocks is $\sim 0.1 R_s$, so that even in young remnants with $R_s \approx 1$ pc the dust is well coupled to the postshock gas.

iii) *Mass of Swept-Up Gas*

The mass of swept-up gas can be directly calculated from the relation $M = 4\pi\rho_0 R_s^3/3$, with R_s determined from equation (23), and $\rho_0 = \mu m_{\mathrm{H}} n_0$. As a consistency check, one can also calculate M indirectly from the mass of the dust necessary to account for the infrared emission. The total mass of radiating dust is given by

$$L_{\mathrm{IR}} = 4 M_d \sigma T_d^4 \langle K(T_d) \rangle\ , \quad (25)$$

where L_{IR} is the total infrared luminosity obtained by integrating equation (14) over the grain size distribution $f(a)$, and M_d is the total mass of the radiating dust. The resulting value of M_d for an MRN mixture of graphite-silicate grains can be written as:

$$M_d(M_\odot) \approx 2 \times 10^5 T_d^{-6} L_{\mathrm{IR}}(L_\odot) \quad (26)$$

which is accurate only to within a factor of ~ 2. The mass of swept-up X-ray emitting gas can be inferred from the infrared emission from the relation:

$$M \approx M_d/(\delta Z_d)\ , \quad (27)$$

where $Z_d \approx 0.0075$ for an undepleted gas of "normal" cosmic abundances.

In the following section I will apply the above relations to derive the plasma conditions, and to calculate the radius and amount of of swept-up interstellar gas for Cas A and the Cygnus Loop.

b) The Cas A Remnant

Cas A is a young remnant, and in their analysis of its infrared emission Dwek *et al.* (1987*a*) considered the possibility that some of the emission may originate from supernova condensed dust that is heated by the reverse shock that travels through the ejecta. Their analysis showed that this possibility cannot be entirely ruled out. However, in the subsequent calculations I will ignore the potential existence of supernova condensates in the ejecta, and attribute all the infrared emission to "ordinary" swept-up interstellar dust. The need to invoke the presence of supernova condensates will arise only if the results of this assumption lead to a major inconsistency with the observations.

The infrared analysis of Cas A suggests that the dust temperature in the remnant is about 90 K, that the total infrared flux from the remnant is 2.4×10^{-8} ergs cm^{-2} s^{-1}, and that the depletion factor (obtained by more detailed calculations than those presented here) is given by $\delta \approx 0.65$. The postshock density of the gas (Fig. 6*b* or 7) is then ~ 10 cm^{-3}, so that $n_0 \approx 2.5$ cm^{-3}. The angular size of Cas A is 2′ (Murray *et al.* 1979), giving a shock radius of 1.62 pc. This gives a distance to the remnant of 2.7 kpc, in excellent agreement with the value of 2.9 kpc that was recently derived by Braun (1987) from the kinematics of the fast-moving knots. The mass of swept-up interstellar gas ($=4\pi\rho_0 R_s^3/3$) is $\approx 1.3\ M_\odot$, in reasonable agreement with the value of 0.4 $M_\odot$ inferred from equations (25) and (26), considering the sensitivity of M_d to the value of the dust temperature. These infrared-derived masses are lower than the value of 3.5 $M_\odot$ derived by Murray *et al.* for the mass of the swept-up X-ray emitting gas. The latter value represents an upper limit on the mass, since nonequilibrium ionization effects in the remnant will lower the amount of gas required to produce the observed X-ray emission by about a factor of ~ 4 (DPSR).

c) The Cygnus Loop

A preliminary analysis of the infrared emission from the Cygnus Loop shows that the average dust temperature is about 33 K, and that the total infrared flux from the remnant is $\sim(8\text{–}16) \times 10^{-8}$ ergs cm^{-2} s^{-1}. The angular radius of the remnant is 84′, and the shock temperature is about 2×10^6 K (Ku *et al.* 1984). For a given dust temperature and gas temperatures below $\sim 2 \times 10^7$ K, the derived gas density depends on the assumed grain size. Figures 6 and 7 show that the postshock density is about 1 cm^{-3} for $a = 0.1$ μm, 0.5 cm^{-3} for $a = 0.05$ μm, and 0.1 cm^{-3} for 0.01 μm sized grains. The density of the ambient medium can range therefore from ~ 0.25 to 0.025 cm^{-3}, depending on the adopted grain size. For comparison, a value of $n_0 \approx 0.16$ cm^{-3} was inferred from the X-ray analysis (Ku *et al.* 1984). The Cygnus Loop is an evolved remnant with an age of $\sim 18 \times 10^3$ yr. Adopting an average grain size $\langle a \rangle = 0.06$ μm (which yields a postshock density of ~ 0.15 cm^{-3}), the dust depletion factor is approximately given by $\delta \approx 0.8$. The derived radius of the remnant is then between 6 to 11 pc, giving an inferred distance of 230–460 pc. This distance represents a lower limit since the infrared morphology of the remnant (Braun 1986) shows that the emission arises from only about 70% of the shell's surface. A more realistic range of values is therefore 330–660 pc. This distance is lower than the commonly accepted value of 770 pc, but in good agreement with the distance of 460 ± 160 pc, recently derived by Braun (1986) from an analysis of the systematic expansion of various diffuse and filamentary features in the remnant.

As a check on the value of the average dust temperature used in the calculations, I will compare the mass of shock-heated gas, derived from equations (26) and (27) for an adopted infrared flux of 16×10^{-8} ergs cm^{-2} s^{-1} and a distance of 770 pc, with that derived from the X-ray observations. The former mass is equal to $\sim 70\ M_\odot$, which is in very good agreement with the estimated value of 100 $M_\odot$ given by Ku *et al.* (1984) for the latter mass. This agreement suggests that the average dust temperature is not too different from ~ 33 K.

VI. SUMMARY

In this paper I presented a detailed analysis of the collisional heating of dust, and of the resulting infrared cooling of the hot plasma. The most important results of this paper can be summarized as follows.

1. The cooling function of a plasma by gas-grain collisions for a gas with a standard gas-to-dust mass ratio was calculated using a new expression for the range of electrons in solids (eq. [3]). The resulting cooling function, presented in Figure 4, is lower by about a factor of 2 from previously published values (e.g., Draine 1981; Dwek and Werner 1981).

2. At temperatures above $\sim 10^6$ K, the cooling of the gas by gas-grain collisions is more effective than its cooling by free-free and ionic/atomic-line emission. For a given dust model and gas-to-dust mass ratio, the ratio of these cooling rates is only a function of gas temperature and is presented in Figure 5. Comparison between the theoretically derived and observed dust-to-gas cooling ratio can yield valuable information on the evolution of a SNR and its interaction with the ambient ISM.

3. The equilibrium temperatures of collisionally heated graphite and silicate grains are presented as a function of grain composition, and plasma temperature and density in Figures 6*a–d*. The dust temperature is weakly dependent on grain composition, and in plasmas with $T \geq 10^7$ K it is weakly dependent on grain sizes as well. Consequently, it should not be surprising that the infrared spectrum of young remnants can be well represented by a single-temperature dust component.

4. Figure 7 presents a diagram depicting contours of constant dust temperatures in the temperature-density (n, T)-plane of the gas. The results show that the infrared spectrum of a hot ($\geq 2 \times 10^7$ K) plasma is primarily determined by gas density and is essentially independent of its temperature. The infrared emission from young remnants can therefore not be used to determine their velocities.

5. If the morphology of the remnant and the postshock dust abundance can be determined with some reasonable degree of accuracy, the infrared observations can be used to determine the remnant's distance and the amount of swept-up interstellar gas (see eqs. [23], [26], and [27]),

6. For Cas A, I derived a distance of ~ 2.7 kpc to the remnant, and a total mass of $\sim 1.3\ M_\odot$ of swept-up interstellar gas. The derived distance is in excellent agreement with that determined from the kinematic study of the fast-moving knots in the remnant (~ 2.9 kpc). The swept-up mass is comparable to that estimated from X-ray emission ($\sim 3.5\ M_\odot$) associated with the forward expanding shock if the latter mass is corrected for nonequilibrium ionization effects.

7. The infrared observations of the Cygnus Loop suggest a distance between 330 and 660 pc, and a total mass of swept-up interstellar gas of $\sim 70\ M_\odot$. These values are consistent with the recently derived distance of 460 ± 160 pc (Braun 1985), and the mass estimate of $\sim 100\ M_\odot$ derived from the X-ray observations (Ku *et al.* 1984).

I thank Dan McCammon for helpful conversations regarding the stopping of electrons in solids, and Rob Petre for running the Raymond-Smith plasma cooling model. This research was supported under NASA's *IRAS* Data Analysis Program and funded through the Jet Propulsion Laboratory.

REFERENCES

Anderson, H. H., and Ziegler, J. F. 1977, *Hydrogen: Stopping Powers and Ranges in all Elements* (New York: Pergamon).
Berger, M. J., and Seltzer, S. M. 1964, *Tables of Energy Losses and Ranges of Electrons and Positrons* (NASA SP-3012).
Braun, R. 1986, *Astr. Ap.*, **164**, 208.
———. 1987, *Astr. Ap.*, **171**, 233.
Burke, J. R., and Silk, J. 1974, *Ap. J.*, **190**, 1.
Dalgarno, A., and McCray, R. 1972, *Ann. Rev. Astr. Ap.*, **10**, 375.
Draine, B. T., and Salpeter, E. E. 1979, *Ap. J.*, **231**, 77.
Draine, B. T. 1981, *Ap. J.*, **245**, 880.
———. 1987, *Princeton Observatory Preprints*, No. 213.
Draine, B. T., and Anderson, N. 1985, *Ap. J.*, **292**, 494.
Draine, B. T., and Lee, H. M. 1984, *Ap. J.*, **285**, 89.
Draine, B. T., and Salpeter, E. E. 1979, *Ap. J.*, **231**, 77.
Dwek, E. 1981, *Ap. J.*, **246**, 430.
———. 1986, *Ap. J.*, **302**, 363.
Dwek, E., Dinerstein, H. L., Gillett, F. C., Hauser, M. G., and Rice, W. L. 1987*a*, *Ap. J.*, **315**, 571.
Dwek, E., Petre, R., Szymkowiak, A., and Rice, W. L. 1987*b*, *Ap. J.* (*Letters*), **320**, L27. (DPSR).
Dwek, E., and Werner, M. W. 1981, *Ap. J.*, **248**, 138.
Graham, J. R., Evans, A., Albinson, J. S., Bode, M. F., and Meikle, W. P. S. 1987, *Ap. J.*, **319**, 126.
Iskef, H., Cunningham, J. W., and Watt, D. E. 1983, *Phys. Med. Biol.*, **28**, 535.
Janesick, J., Elliott, T., and Garmire, G. 1985, *SPIE on X-Ray Instrumentation in Astrophysics*, 1.
Ku, W., H.-M., Kahn, S. M., Pisarski, R., and Long, K. S. 1984, *Ap. J.*, **278**, 615.
Low, F. J., *et al.* 1984, *Ap. J.*, **278**, L19.
Marsden, P. L., Gillett, F. C., Jennings, R. E., Emerson, J. P., de Jong, T., and Olnon, F. M. 1984, *Ap. J.* (*Letters*), **278**, L29.
Mathis, J. S., Rumpl, W., and Nordsieck, K. H. 1977, *Ap. J.*, **217**, 425 (MRN).
McKee, C. F. 1974, *Ap. J.*, **188**, 335.
Mezger, P. G., Tuffs, R. J., Chini, R., Kreysa, E., and Gemund, H-P. 1986, *Astr. Ap.*, **167**, 145.
Mufson, S. L., McCollough, M. L., Dickel, J. R., Petre, R., White, R., and Chevalier, R. A. 1986, *A.J.*, **92**, 1349.
Murray, S. S., Fabbiano, G., Fabian, A. C., Epstein, A., and Giacconi, R. 1979, *Ap. J.* (*Letters*), **234**, L69.
Ostriker, J. P., and Silk, J. 1973, *Ap. J.* (*Letters*), **184**, L113.
Puget, J. L., Leger, A., and Boulanger, F. 1985, *Astr. Ap.*, **142**, L19.
Raymond, J. C., Cox, D. P., and Smith, B. W. 1976, *Ap. J.*, **204**, 290.
Seab, C. G. 1986, in *Interstellar Processes*, ed. D. Hollenbach and H. A. Thronson, Jr. (Reidel: Dordrecht), p. 491.
Sedov, L. I. 1959, *Similarity and Dimensional Methods in Mechanics* (New York: Academic Press).
Shull, J. M. 1977, *Ap. J.*, **215**, 805.
Silk, J., and Burke, J. R., 1974, *Ap. J.*, **190**, 11.
Spitzer, L. 1968, *Diffuse Matter in Space* (New York: Interscience), p. 146.
Taylor, G. I. 1950, *Proc. Roy. Soc. London*, **A201**, 159.
Watson, M. G., Willingdale, R., Pye, J. P., Rolf, D. P., Wood, N., Thomas, N., and Seward, F. D. 1983, in *IAU Symposium 101, Supernova Remnants and Their X-Ray Emission*, ed. J. Danziger and P. Gorenstein (Reidel: Dordrecht), p. 273.
Weiland, J., Blitz, L., Dwek, E., Hauser, M. G., Magnani, L., and Rickard, L. J 1986, *Ap. J.*, **306**, L101.

ELI DWEK: Code 685, NASA Goddard Space Flight Center, Greenbelt, MD 20771